Journal of Natural Gas Science and Engineering 108 (2022) 104834

Contents lists available at ScienceDirect

Journal of Natural Gas Science and Engineering

journal homepage: www.elsevier.com/locate/jngse

Fines effect on gas flow in sandy sediments using μCT and pore networks

Jamal A. Hannun [a], Riyadh I. Al-Raoush [a,*], Zaher A. Jarrar [b], Khalid A. Alshibli [b], Jongwon Jung [c]

[a] Department of Civil and Architectural Engineering, Qatar University, P.O Box 2713, Doha, Qatar
[b] Department of Civil & Env. Engineering, 325 John Tickle Building, University of Tennessee, Knoxville, TN, 37996, USA
[c] School of Civil Engineering, Chungbuk National University, Cheongju, Chungbuk, 28644, Republic of Korea

ARTICLE INFO

Keywords:
Fines clogging
Pore network
Multiphase flow
Sandy sediments
Micro-computed tomography
Methane hydrate

ABSTRACT

Gas production from hydrate-bearing sediments requires methane dissociation, which induces two-phase gas flow, mobilizing fine clay particles from within saturated pores. Fines migration within sandy sediments results in subsequent pore clogging, reducing reservoir connectivity. Sediments complex pore morphology, require direct 3D microscopic pore-scale imaging to investigate fines' influence on the porous media. The work uses synchrotron microcomputed tomography, to understand how fines migration due to gas injection, affects pore morphology and gas connectivity within sandy sediments. The goal is to study the impact of fines type and content at different gas injection stages, on gas flow regime and sediments rearrangement.

Six saturated samples of sand and fines mixtures (Kaolinite and Montmorillonite at different contents) underwent four stages of gas injection during in-situ 3D scanning. X-ray images were segmented for direct visualization, as well to quantify gas ganglia distribution, also to extract pore networks to statistically measure changes in pore and throats distributions, and to simulate single-phase and relative permeability.

Findings reveal that the extent of deformation to pore morphology increases with fines content and gas injection regardless of fines type. High kaolinite content (equal to or larger than 6%) results in fractured porous media, while high montmorillonite content (equal to or larger than 5%) results in disconnected vuggy media. Lower contents cause a gradual reduction in pore and throat sizes during gas injection. As fines content increases, clogging intensifies, thus gas connectivity and flow regime changes from connected capillary to disconnected vugs and microfractures. Both hydrophobic and hydrophilic fines reduced throat sizes, due to dislocations in sand grains. A unique pattern is discovered using pore networks, which describe pore-size fluctuations during fractures and vugs formation, due to fines migration.

1. Introduction

Reserves of Methane Hydrate are three times larger than all other fossil fuels combined (Klauda and Sandler, 2005), with volume estimates of over quadrillion cubic meters according to (Milkov, 2004). Pilot projects demonstrated economic feasibility and the potential for CH_4–CO_2 replacement in unconsolidated sandy reservoirs (Schoderbek et al., 2013; Kvamme, 2015; Merey et al., 2018). Hydrates form in marine environments, at high pressure and low temperature within deposits of saturated unconsolidated sandy sediments (Mrozewski et al., 2011; Boswell et al., 2012; Cook and Malinverno, 2013), mixed with fine clay particles (Kajiyama et al., 2017). When hydrate dissociates during production, gas travel from within the pores, displacing seawater; the generated hydrodynamic forces and the sweeping motion of the gas-brine interface are major mobilizers of fine clays. In sandy reservoirs, fines comprise less than 10% of sediments' weight (Muecke, 1979). Fines which are classified as hydrophilic (water-swelling), are commonly observed at the brine-gas interface, such as montmorillonites; while hydrophobic (non-swelling) fines, naturally attach to both brine-gas and sand-brine interfaces, such as kaolinites (Deer et al., 1992; Jung et al., 2018a). During fines migration, particles larger than the throat clog the pore network (Hannun et al., 2020), causing a pressure build-up that can dislocate sand grains in unconsolidated media (Khan et al., 2017).

Fines migration and subsequent clogging reduce reservoir porosity and permeability (Song and Kovscek, 2016; Prempeh et al., 2020; Guo et al., 2022), causing formation damage that costs the hydrocarbon industry $140 billion/year (Byrne, 2012). Clogging depends on fines type

* Corresponding author.
E-mail address: riyadh@qu.edu.qa (R.I. Al-Raoush).

https://doi.org/10.1016/j.jngse.2022.104834
Received 3 August 2022; Received in revised form 30 September 2022; Accepted 31 October 2022
Available online 3 November 2022
1875-5100/© 2022 The Authors. Published by Elsevier B.V. This is an open access article under the CC BY license (http://creativecommons.org/licenses/by/4.0/).

and content, gas flow rate and pore morphology (mainly pore and throat sizes, along (o/d) ratio of throat to fine particle size). Migration and clogging of fines undergoing single and multiphase phase flow were explored using microfluidic models (Bizmark et al., 2020; Jang et al., 2020; Nishad et al., 2021), 3D tomography (Lagasca and Kovscek, 2014; Khan, 2016; Al-Raoush et al., 2019), core flooding (Coronado and Díaz-Viera, 2017; Russell et al., 2017; Prempeh et al., 2020), and numerical simulations (Samari Kermani et al., 2020; Parvan et al., 2021; Elrahmani et al., 2022). Microfluidics are useful in isolating parameters but cannot simulate sediments' roughness or pore morphology. Tomography is a robust non-destructive technique to reconstruct samples, but compromises sample sizes to resolution. Core flooding provides benchmarks for in-situ samples with the ability to control a wide range of physiochemical variables but lacks in accessing direct pore-scale observations. Simulations are an efficient method to predict pore-scale physics but compromise accuracy to reduce computational cost.

Synchrotron X-ray microcomputed tomography (SMT) can reconstruct 3D volumes of sand, uncovering pore morphology at a microscopic level. Synchrotron radiation with high brilliance and tunable energy, is suitable for scanning multiphase flow experiments, through unconsolidated sand at a quasi-static state. Also, varying fines content in the study is important, as content increases radially in the subsurface when approaching a production well. CO_2 injection coupled with fines contents above 4% (by weight of sand), can cause fractures in sediments (Jung et al., 2012a), which is critical to the borehole's stability in hydrate-bearing sediments. Pore networks can be extracted using spatial information from SMT 3D images, facilitating multiphase flow simulation to measure the effect of pore morphology change on relative permeabilities of the sediments (Finlay et al., 2014; Solling et al., 2014; Golparvar et al., 2018).

There is a rising need to understand the effect of fines migration and clogging on pore morphology and gas flow connectivity, especially at the pore scale in unconsolidated sandy sediments. Thus, using 3D microcomputed tomography (μCT) is essential to model and quantify the influence of fines on multi-phase flow within sandy sediments. The objectives are to:

(i) investigate the effect of clay type among kaolinite and montmorillonite, using gas ganglia analysis and 3D visualization from synchrotron micro-computed tomography (SMT);
(ii) understand how changing fines content between 2% and 6% will influence fines migration and clogging, by utilizing pore networks to quantify changes in pore morphology during gas injection in saturated loose sand;
(iii) gauge the effect of CO_2 gas injection on fines migration, clogging, gas-induced vugs and fractures, using pore networks and gas relative permeability simulation.

The experiments employ samples with 2 types of fines, with 3 different contents for each type, each sample undergoes 4 steps of gas injection, to study the effect of fines on pore space and multiphase flow in sandy porous media.

2. Methodology

2.1. Materials

F75 silica sand with grain sizes between 0.250 mm and 0.210 mm was used in the experiments (obtained from US Silica Company). The sand is hydrophilic and has a specific gravity of solids (Gs) of 2.65, a rounded shape with sphericity and roundness of 1.55 and 0.89, respectively, calculated using the procedure of (Alshibli et al., 2015). The uniformity and conformity coefficients measured using the method of (Al-Raoush, 2012) were found to be 1.40 and 1.02, respectively. Kaolinite and montmorillonite were the fine clay particles used (sourced from Vanderbilt Minerals Company). The fines have flaky shaped particles, and a Gs of 2.62. with a mean particle size of 0.6 μm. Kaolinite is a hydrophobic non-swelling clay, while montmorillonite is a hydrophilic water-swelling clay. Fines were mixed with sand at different percentages by weight to replicate fines migration mechanisms from within subsurface reservoirs (Crist et al., 2005; Kajiyama et al., 2017). The dry sand-fine mixtures were prepared in six proportions as presented in Table 1. The fines content ranged between 2% and 6% for kaolinite, and between 2% and 5% for montmorillonite.

Critical fines content (FC*) is the content of the fine that completely fills the pores of sandy sediments, where fines content is the ratio of the weight of fines (w_f) to sand weight (w_c). Park and Santamarina (2017) used the gravimetric-volumetric analysis to reveal that FC* is a function of the void ratio of sand (e_c) and fines (e_f) as given in Eq. (1):

$$FC^* = \frac{w_f}{w_c} = \frac{e_c}{1 + e_c + e_f} \quad (1)$$

Since the void ratio of sand ($e_c = 0.67$), therefore, FC* is 9% for montmorillonite ($e_f = 5.4$) and 21% for kaolinite ($e_f = 1.5$), because the critical fines content decreases as the plasticity of fines increases. Jung et al. (2012b) showed that at a fines content above 4%, fines migration can cause clogging in pores which can result in vugs and fractures during gas production in hydrate-bearing sediments, while Jarrar et al. (2019) showed that at 6%, fines migration and fracturing occur. No confining stress is required for the experiments because for both 6% kaolinite and 5% montmorillonite, the contents are well below the FC*, thus fines will not carry the effective stress load.

The samples were prepared by collecting a fraction of F75 sand with sizes between sieve #60 and sieve #70. The sand was then rinsed with distilled water and oven-dried. Then, the sand was divided into six patches where each patch was mixed with kaolinite or montmorillonite clay powder. The goal was to prepare sand-clay mixtures with the same porosity and fines contents as given in Table 1.

Each mixture was loosely packed in an acrylic cylinder. The acrylic cylinders have an internal height and diameter of 50.80 mm and 9.52 mm respectively. The packing method mimics sandy sediments in saturated marine environments, formed by the deposition of sequential beds on top of each other, due to the sedimentation process. Thus, five sequential layers of sediments were placed on top of each other to fill the brine-saturated cylinder. Initially, the cylinder was partially filled with brine (2% KI de-aired water solution) and then deposited equal amounts of sediments in five layers. More brine was added after each deposited layer to accommodate the mixture until all five sediment layers were packed (Al-Raoush et al., 2019). Each of the six cylinders contained 4 g of sand with (0.8 g, 0.16 g, 0.24 g) of kaolinite and (0.8 g, 0.12 g, 0.20 g) of Montmorillonite. These values correspond to 2%,4%, 6% and 2%, 3%, 5% fines contents, respectively. The volume fractions of sand, fines and brine were calculated to achieve a target porosity of 40%, using soil-phase relationships.

2.2. Experimental setup

Fig. 1-a shows the experimental setup used to conduct the fines migration experiments at Beamline 13D of the Advanced Photon Source (APS) at Argonne National Laboratory (ANL), Illinois, USA. The top and bottom of the cylindrical columns were plugged with filters and glass beads. The bottom port was connected to a CO_2 gas cylinder and a

Table 1
Types and contents of fines as ratio of sand weight, 3 cylinders contain kaolinite fines which are hydrophobic non-water swelling, the other 3 cylinders contain montmorillonite fines which are hydrophilic water swelling, oven dry sand and fines were mixed before packing into each cylinder.

Fines Type	Fines Contents (% of sand weight)		
Kaolinites (K)	2%	4%	6%
Montmorillonites (M)	2%	3%	5%

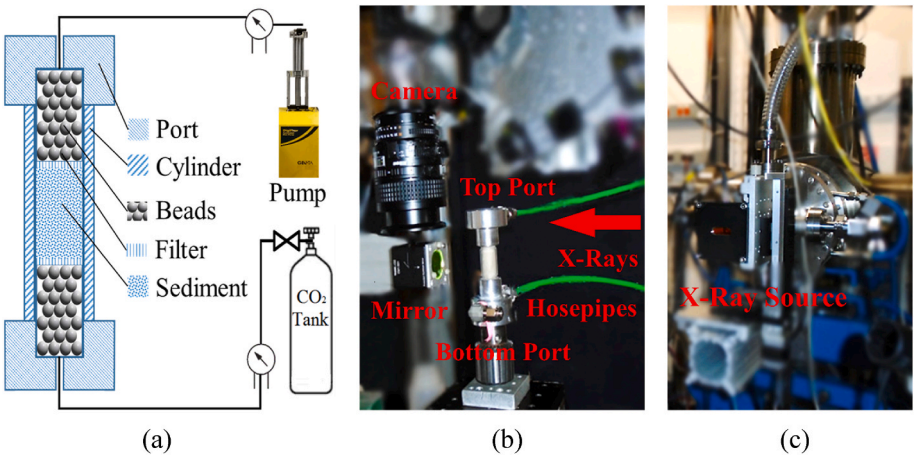

Fig. 1. Experimental setup at ANL APS, (a) a sketch of the experimental setup; (b) specimen is placed vertically to take 360º x-ray projections; (c) the beam source from the synchrotron ring.

pressure regulator, while the top port was connected to a pressure-volume actuator (DigiFlow pump). The glass beads assist in transitioning the flow from upper and lower ports, toward the sediments in the cylinder by distributing streamlines parallelly. Filters were used to prevent fines from flowing toward the flow pump or the pressure regulator. Fig. 1-b shows the sample placed vertically on a rotating stage where a camera captures the x-ray projections as the sample rotates 360°, while Fig. 1-c shows the x-ray beam source diverted into the experimental hatch, from the storage ring at APS.

2.3. Scanning stages

X-ray μCT is a robust non-destructive imaging technique that collects projections of a rotating sample to reconstruct the 3D internal volume. An enhancement to laboratory-based μCT is a synchrotron radiation source that has the advantages of high brilliance and tunable energy levels, allowing to reconstruct volumes of dense materials like sand with high contrast and lower noise (Al-Raoush et al., 2019).

Salt of Potassium Iodide (KI) was dissolved in distilled water at a concentration of 2% by water weight to function as a doping agent, enhancing the brine phase contrast and facilitating image segmentation. The dissolved KI does not impact brine properties as other studies used higher concentrations with minimal differences in properties (Iglauer et al., 2013; Andrew et al., 2014). Dual Energy Computed Tomography (DECT) is used to scan the samples twice at different x-rays energy levels, below and above the iodine K-edge, 33.069 keV and 33.0269 keV respectively. DECT technique is effective in increasing image contrast, limiting the effects of noise and allowing for accurate isolation of the brine phase within the pores, which results in better features detection when selecting the CT Number range (intensity value) during segmentation, ensuring enhanced identification and separation of the different phases in the system (fines, sand, brine, gas). The scans have a resolution of 3.89 μm^3/voxel, the volume of each scan is 1920 × 1920 × 2356 voxels or about 7.5 × 7.5 × 9.2 mm (Jarrar et al., 2020).

Six samples containing different fines contents were prepared, imaged and analyzed at four different stages each. Fig. 2 shows cross-sections obtained from 3D images showing the four CO_2 gas injection stages, initially the sample was fully saturated at stage 1; then stage 2 was established when CO_2 was injected at 27.6 kPa pressure replacing 0.4 ml of brine; next additional 0.6 ml of brine was withdrawn at stage 3; finally gas pressure was increased to 41.4 kPa at stage 4. The pump withdrew brine from the top port, allowing for gas to percolate through the sample, flow was paused and for each stage, the sample was scanned at a quasi-static state. Fig. 2-b shows a microfracture forming in the 6% kaolinite sample, where gas flow causes fines to clog the throats, building up pressure, and displacing sand grains. All images were

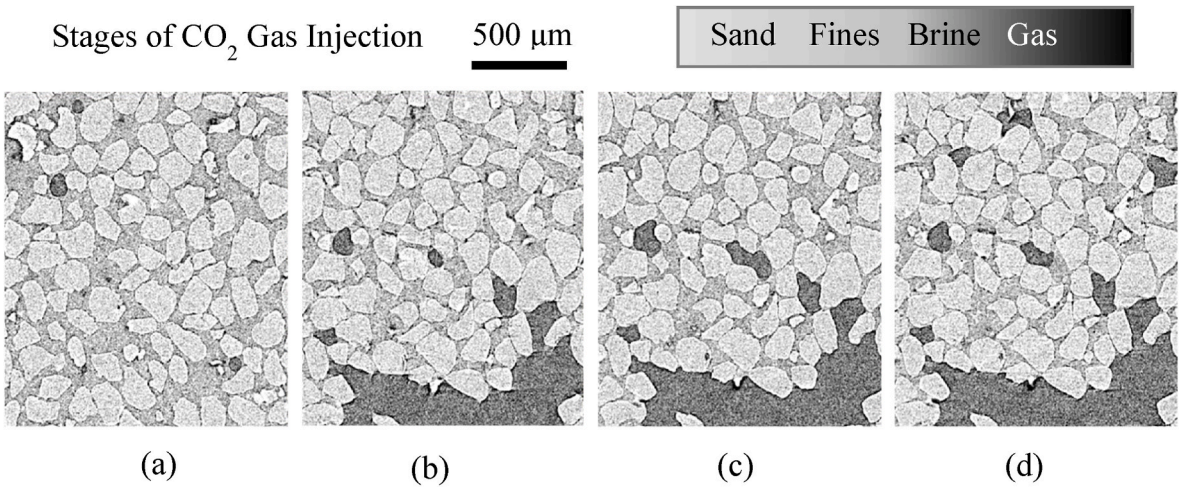

Fig. 2. Cross sections obtained from 3D images showing CO_2 gas injection stages, (a) initial fully saturated sample of stage 1; (b) CO_2 is injected at 27.6 kPa pressure replacing 0.4 ml of brine at stage 2; (c) additional 0.6 ml of gas is injected at stage 3; (d) gas pressure is increased to 41.4 kPa at stage 4; at (b) during stage 2 a gas fracture of the 6% kaolinite sample is shown, gas is observed mobilizing the sand grains.

scanned at the middle of the samples not covering the cylinder's full height. Thus, multi-step scanning was conducted to ensure that any change in pore morphology is captured. For consistency, this procedure was adopted for all samples.

2.4. Image analysis

All image analysis was carried out using the built-in algorithms of Pergeos software (FEI, 2020) by (Thermo Fisher Scientific). Fig. 3-a displays a raw grayscale image with the corresponding histogram shown in Fig. 3-d. It illustrates the random distribution of noise in the images which in turn reduces the clarity of the images. The initial step in post-processing tomography images was to reduce data noise through image filtration. The filtration was done using Anisotropic diffusion followed by Median filters. Anisotropic diffusion filter utilized the raw image with an isotropic Gaussian filter that blurs the noise inside of each phase, while edges with large differences (contrast) in grayscale were preserved, hence the name of anisotropic diffusion (Malik and Perona, 1990). Then, a median filter was applied to reduce image contrast using a low pass filter that attenuates high frequencies, making each phase more distinct from the previous image as demonstrated in Fig. 3-c. The median filter (Pratt, 2014) replaces the value of each voxel with the median value of the 26-neighboring voxels in three iterations.

After filtering the raw grayscale image and removing noise and artifacts as shown in Fig. 4-a and Fig. 4-b, voxels intensities (CT Number) redistribute to reflect the material phases within 3D images as illustrated in Fig. 4-d and Fig. 4-e. Segmentation was done by selecting voxels within a specific CT Number range for each material and assigning it to a distinct value. An interactive overlay threshold tool in Pergeos software was used to serve this purpose. Then, a range of intensities was selected and the corresponding voxels were overlaid to check the accuracy of the selection. At each gas injection stage, the DECT technique was employed by acquiring two images with higher and lower energy levels (above and below the Iodine edge). Images below the Iodine edge were used to segment sand and voids, while images above the Iodine edge facilitated gas segmentation, whereas the image difference was used for brine phase segmentation (Ham et al., 2004). For sand-kaolinite samples, voxels below −150 CT Number were labeled as the gas phase, whereas voxels below −200 CT Number for sand-montmorillonite samples were labeled as the gas phase. The selected voxels were given a value of 1, representing the first phase. Values above −150 and below 25 CT Number were assigned as brine for the kaolinite samples; while for the montmorillonite, a range between −200 and 0 CT Number represented brine and was allocated a value of 2. Fines were segmented using the method of Jarrar et al., 2020 who demonstrated that in similar systems, fines can be extracted from the change in voxels intensity. DECT was used to isolate fines using density variation resampled in voxels CT Number, by conducting arithmetic operations on images of high and low energy levels. The operation was employed over cubical REV regions to overcome local intensity changes (Jarrar et al., 2021). This was done only to observe the fines' location through the DECT technique. Later in the analysis, fines will be allocated to brine to study gas disconnections and the change in pore morphology through pore networks. Fines phase in the kaolinite and montmorillonite were respectively selected as 25 to 125 CT Number and 0 to 150 CT Number, then assigned a value of 4. The sand phase was selected with values larger than 125 CT Number for the kaolinite and 150 CT Number for the montmorillonite column as illustrated by the largest peek in Fig. 4-f.

Following image segmentation, pore networks were generated followed by single and multiphase permeability simulation. Finally, variation in gas ganglions due to the presence of fines with different contents and types was quantified., separate gas ganglia were given distinct labels to quantify ganglia volume distribution in each system (shown as different colors in Fig. 13).

3. Results and discussion

3.1. Pore morphology

The gradient of capillary pressure within microscale pores in sediments dominates the mass transport, hence, the capillary pressure equation governs the multi-phase flow at the reservoir scale. The

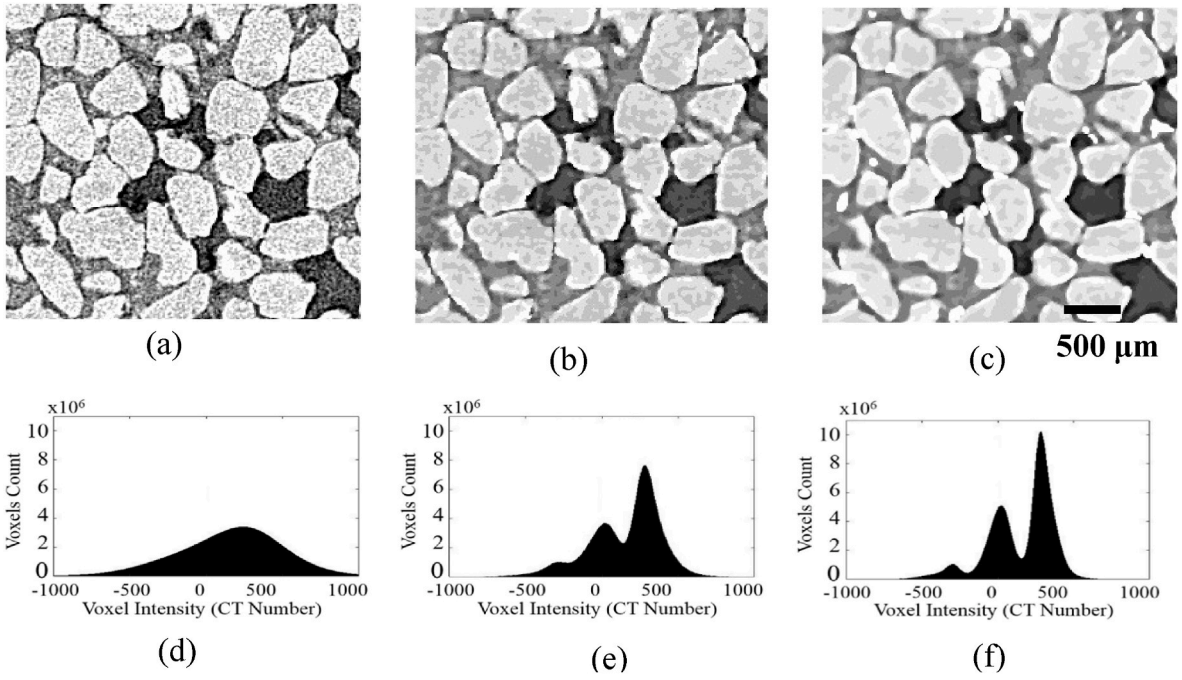

Fig. 3. Sample of filtration showing image and the corresponding histogram, (a) raw grayscale section before filtration, while (d) the corresponding histogram for the intensity values of voxels in the raw 3D image. (b) and (e) demonstrates the effect of the Anisotropic diffusion filter on the image and distribution of intensity values, noise inside of each phase is filtered while edges with high contrast are preserved. (c) and (f) depicts how the median filter attenuates high frequencies using voxels median CT Number making each phase more distinct than the previous image.

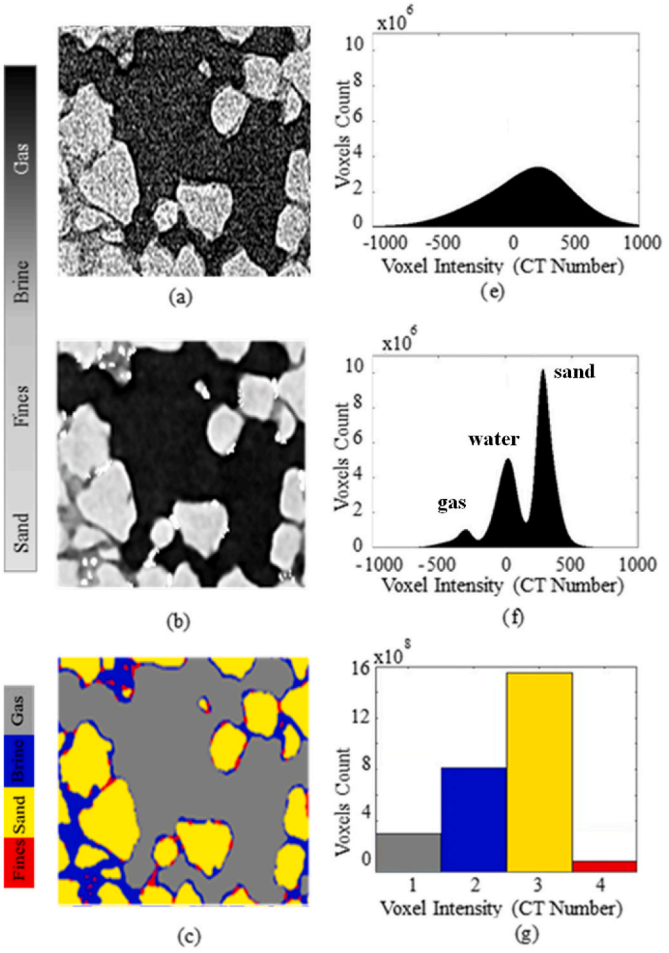

Fig. 4. Filtration and segmentation of a 3D raw image. (a) Raw image, (b) filtered image, (c) segmented image showing different phases in the system, (e) histogram of raw image, (f) histogram of the filtered image showing different phases that have been isolated, (g) phases are segmented to gas (gray), water (blue), sand (yellow), fines (red).

capillary pressure can be calculated from the following capillary pressure relation:

$$P_c = \frac{2\sigma \cos\theta}{R} \tag{2}$$

where P_c is the capillary pressure, σ is the interfacial tension between fluids, θ is the contact angle, and R is the pore-throat radius. Eq. (2) demonstrates that the most effective spatial geometrical predictor of capillary pressure is the radius of the pore-throat where multi-phase flow occurs. Thus, the complex geometry of the pore morphology can be simplified using pore networks (Al-Raoush and Willson, 2005; Oren et al., 2007). Pore networks are used to fill an irregular pore space with simple spheres (pores) and connecting cylinders (throats). A pore network was generated for the samples at each gas injection stage, to understand how the CO_2 flow changed the pore network statistics of the system, and to conduct flow simulation and quantify the change in permeability. A sample of a generated pore network is shown in Fig. 5.

Fig. 5 illustrates a pore network generated using a grain-based algorithm (Bakke & Øren, 1997, 2002). The algorithm only uses the 3D geometry of the void space, starting by constructing a skeleton of the central line of the porous media, then the intersection points are grown to spheres in 3D. Then, the inscribed sphere radius increases until a sand grain is contacted. Grain-based algorithms are documented to be the most suitable to model unconsolidated sand samples, with minimum overlap with the sand grains compared to other methods (Xiong et al., 2016). Additionally, the generated pore network only consists of simple spheres and connecting cylinders representing the governing morphological parameter (radius) which controls the flow through sandy sediments. This method results in a simple model that can be used to perform efficient computer-based flow simulation experiments. Fig. 5-d demonstrates how the model is effective in fitting spheres and cylinders to the exiting pore space. The fractured system of 6% kaolinite represents a critical case where a fractured throat has a radius similar to pores, which is an accurate simplification for a fractured region, demonstrating the capability of gauging changes in pore morphology for the sandy porous media in this study.

Fig. 6 shows the distribution of throat radii for all 24 generated pore networks. Generally, as fines content increases, the extent of deformation to pore morphology increases as gas flow induces fines migration. Also, higher fines contents result in skewing the distribution toward lower throat sizes and higher throat numbers, indicating that throats get divided due to fines migration and clogging. For instance, in the 4% kaolinite sample, as more gas is injected from stage 1–4, the radius mode declined from 17 μm to 13 μm, with throats counts rising from 16 thousand to 18 thousand throats. Indicating that throats constricted and were split changing the pore network morphology due to gas injection. For applications such as hydrates production, where low confinement pressure is expected, CO_2 gas injection or the release of natural gas can displace fines, clogging the throats, resulting in the dislocation of sand grains, which is characterized by the change in the pore morphology in Fig. 6. Such effect starts from 4% kaolinite (>0.19FC*) and 3% montmorillonite (>0.33FC*). More importantly, as the throat size to fine particle size decreases with CO_2 injection, more clogging occurs. Besides, throat radius distribution is bimodal throughout gas injection at 2% content. Yet changing gradually from bimodal to unimodal during injection at 3–4%. At 5–6% the change to unimodal occurs at the first instant of gas injection, the fluids interface sweeps highly concentrated fines thus clogging throats, altering pore morphology majorly toward smaller throats while opening few large flow pathways.

Fig. 7 uses pore network statistics to gauge the effect of sand movements during gas injection over different fines types and contents. Fig. 7-a shows that at low to middle fines content (<0.28FC* for kaolinite and <0.55FC* for montmorillonite), the mean radius of the throats gradually declines. While in samples with high fines content, a rapid fall in throat radii is observed at the first gas injection in stage 2, then as additional gas enters the sample in stage 3 a rapid radii increase is seen. Followed by a decline when gas pressure is raised at the last stage, while Fig. 7-b exhibits an identical behavior for throat lengths along with Fig. 7-c for pores radius. Having multiple columns (6% kaolinite and 5% montmorillonite) confirms that this unique pattern is due to fines, which are observed for the first time and of substantial scientific value. The coordination number in Fig. 7-d, is the number of throats attached to a pore, where the mean value was around 6 for all samples, dropping to 5 temporarily upon gas injection in sediments with high fines content.

But returning to 6 as injection continues. No universal relation was detected for the change in mean coordination number over the steps of gas injection at different fines contents, this might be caused by the large number of pores in the sample, normalizing insignificant changes at the system level. This experimental finding of the change in average coordination number of pores due to sand displacement under hydrodynamic forces is consistent with CFD-DEM simulations where dislocations in sand arches and skeletons were studied and a fluctuation of coordination number was observed (Song et al., 2021).

Fig. 8-a presents the change in the number of throats per system while Fig. 8-b is for the number of pores. The 4% kaolinite and 3% montmorillonite samples show a steady upsurge in the count, while the 6% kaolinite and 5% montmorillonite samples exhibit a rapid rise then a fall followed by a systematic rise. This is caused by sudden movements of sand grains that divided pores and throats, thus raising the count. In the majority of samples, as gas flows and mobilizes fines, the throats number

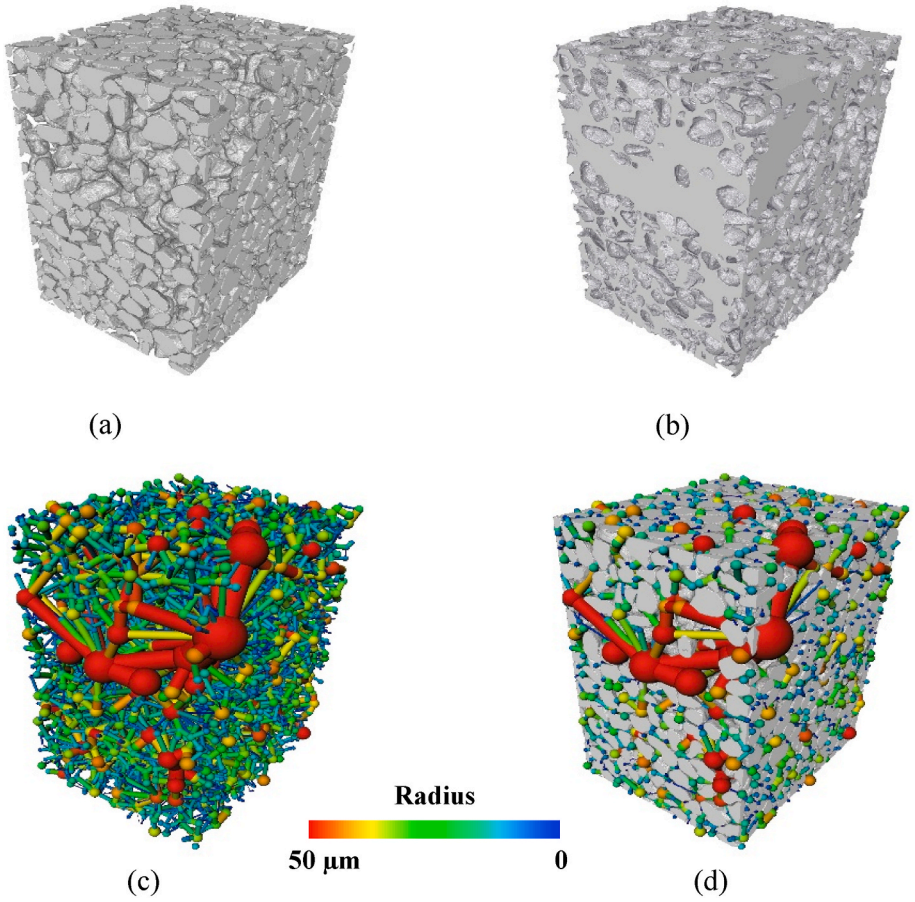

Fig. 5. A cut from kaolinite 6% stage 4, (a) sand grains, (b) pore space, (c) pore network, (d) sand grain and pore network.

increases due to settlement because of sediments' consolidation. Fig. 8-c demonstrates that permeability declines as more gas enters the samples. Not including the 6% kaolinite sample (with the highest fines content), because a fracture developed. Thus, as more gas is injected, the fractured aperture widens, therefore, increasing the permeability, Han et al. (2018) found that if 1% of fines leaves the system, permeability can improve by 30% in hydrate-bearing sediments, which agrees with the results. However, the 5% montmorillonite system had a decrease in permeability followed by a slight increase, which is due to a drop in throat radius. These findings agree with studies that found that hydrophilic fines can detach gas ganglions (Wan and Wilson, 1994), while hydrophobic fines cause fractures in unconsolidated sand (Jarrar et al., 2020).

Next, two-phase flow through pore networks is simulated to generate relative permeability curves using the model of (Ruspini et al., 2017). The flow simulation uses the network geometry and the media contact angles (15°–35°), along with fluids properties like density, interfacial tension (0.07 N/m) and flow direction to simulate drainage and imbibition. For the 4% kaolinite sample (Fig. 9), as gas injection stages develop from 1 to 4, water relative permeability (krw) increases by 5% while the gas relative permeability (krg) declined, suggesting that as more gas flows in the unconsolidated media, the krg is reduced for water flooding experiments. The latter point was observed by (Xiong et al., 2016), where maximum krg dropped as pore morphology shrank and fines content increased. The model accuracy was validated by the variation in irreducible gas saturation after flooding the pore space in Fig. 9, which changes from water saturation of 0.82 to 0.7 between initial and final stages due to fines migration, which agrees with the labeled images results from the tomography experiments.

Moreover, Fig. 10 illustrates the montmorillonite 5% sample drainage simulation. Near 0.9 water saturation (Sw), an upsurge is observed for krw by 25% from the first gas injection stage. This complements the observed increase in relative permeability of gas (krg) between Sw = 0.3 to 0.1 (corresponding to the first pore morphology change). Additionally, at 0.5 Sw, krg is found to rise gradually as stages develop from 1 to 4. Therefore, the combined effect of fines and CO_2 injection on sand dislocations and the corresponding change to pore morphology was evaluated using pore networks and relative permeability simulations. Next, the effect of fines type and content, on the distribution of the non-wetting gaseous phase will be discussed.

3.2. Gas flow connectivity

Fig. 11 illustrates a direct observation of 3D sections from the tomography, the 6% kaolinite sample (left), the hydrophobic kaolinite fines are observed at both the sand-brine and brine-gas interface, while for the 5% montmorillonite sample (right), the hydrophilic montmorillonite fines are observed mainly at the brine-gas interface. This agrees with observations made by (Jung et al., 2018) on microfluidic models on brine-gas interface sweeping. The fluids interface is the most important mobilizer of fines from within the pores toward a production well (Bate et al., 2022). This also agrees with Nishad et al. (2021) work that utilized standard latex microspheres and water wet glass micromodels, where the majority of particles were hosted within the water phase, however 3.4% of hydrophobic particles in the system were retained on gas-water interface compared to 34.5% for hydrophilic particle, at a pH of 7 and low salinity. While after drainage both particle types retain about 50% of the remaining fines in the system on the gas-water interface.

Fig. 12 displays a 2D vertical section of all samples after the final stage of gas injection. It is evident from the images how the gas invaded

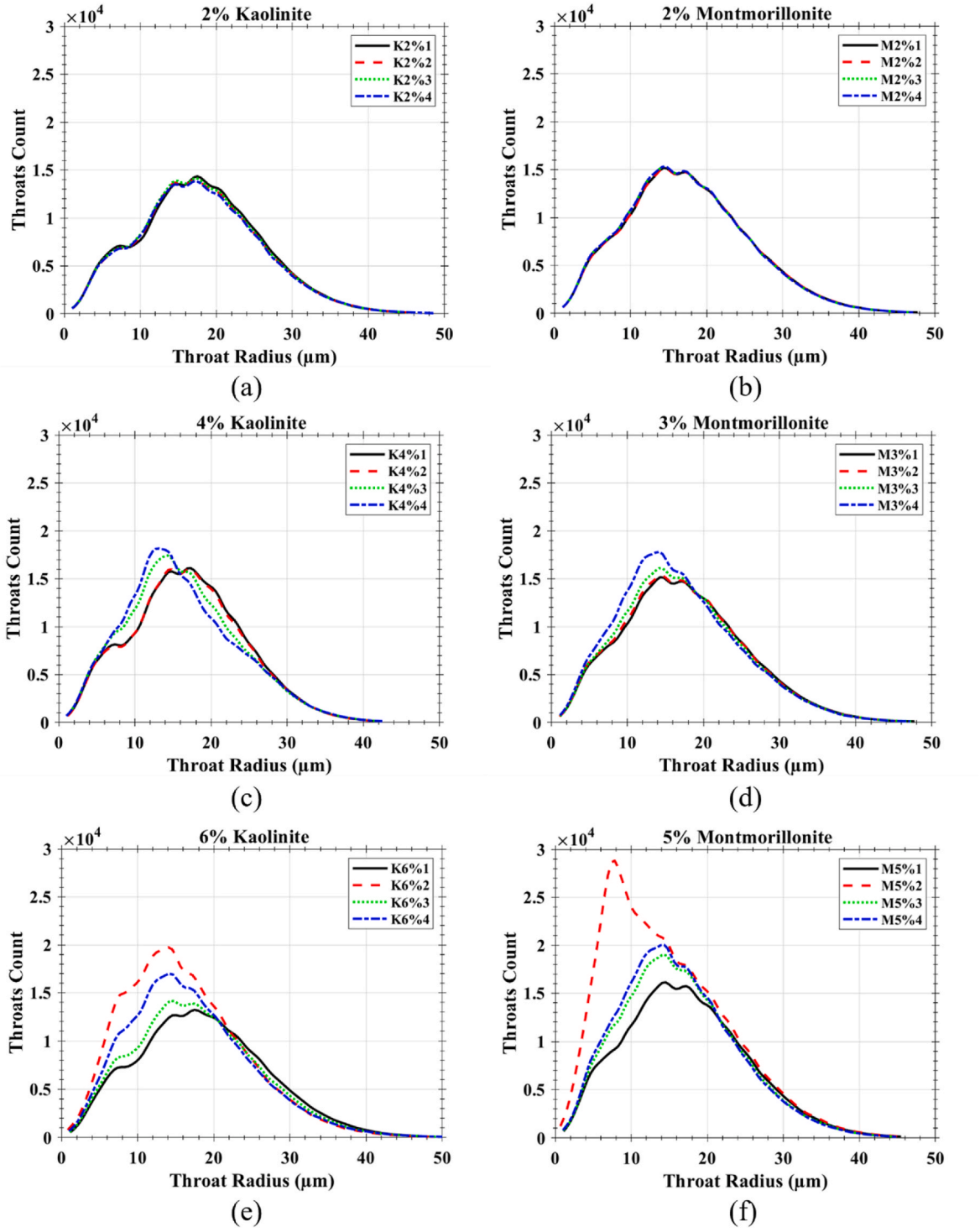

Fig. 6. Distributions of throat radii for all systems at CO_2 injection stages from 1 to 4, higher fines content results in skewing the distribution toward lower throat sizes.

many small pathways that are distributed all over the sections of K2% and M2%, as well for K4% and M3% where gas percolated in more pathways. However, a gas-driven fracture developed at K6%, when fines content increased, phenomena like throat clogging causes gas pressure to increase locally mobilizing grains. The figure shows a noticeable dislocation of the grains opening the main path for gas flow. It is noted that because of throat clogging, there is no percolation of the gas other than the main branch of the fracture. The sand fracture in K6% can open space for more gas volume to flow, increasing the permeability, which justifies the permeability jump in Fig. 8-c. Moreover, Fig. 12-M5% displays the formation of vugs which agrees with Khan et al. (2020) observations on the increase in vugs sizes due to fines migration. In addition, Jung et al. (2018) observed that in sandy sediment cores, undergoing hydrate dissociation, at a fines content of 5%, vugs start forming, while at 6% fractures occur. Such phenomena were theorized by Jung et al. (2018), as the gas-brine interface sweeps fines from within the media during drainage (due to surface charge and capillary effects), the content of fines on the interface surfaces increases, as well as the gas

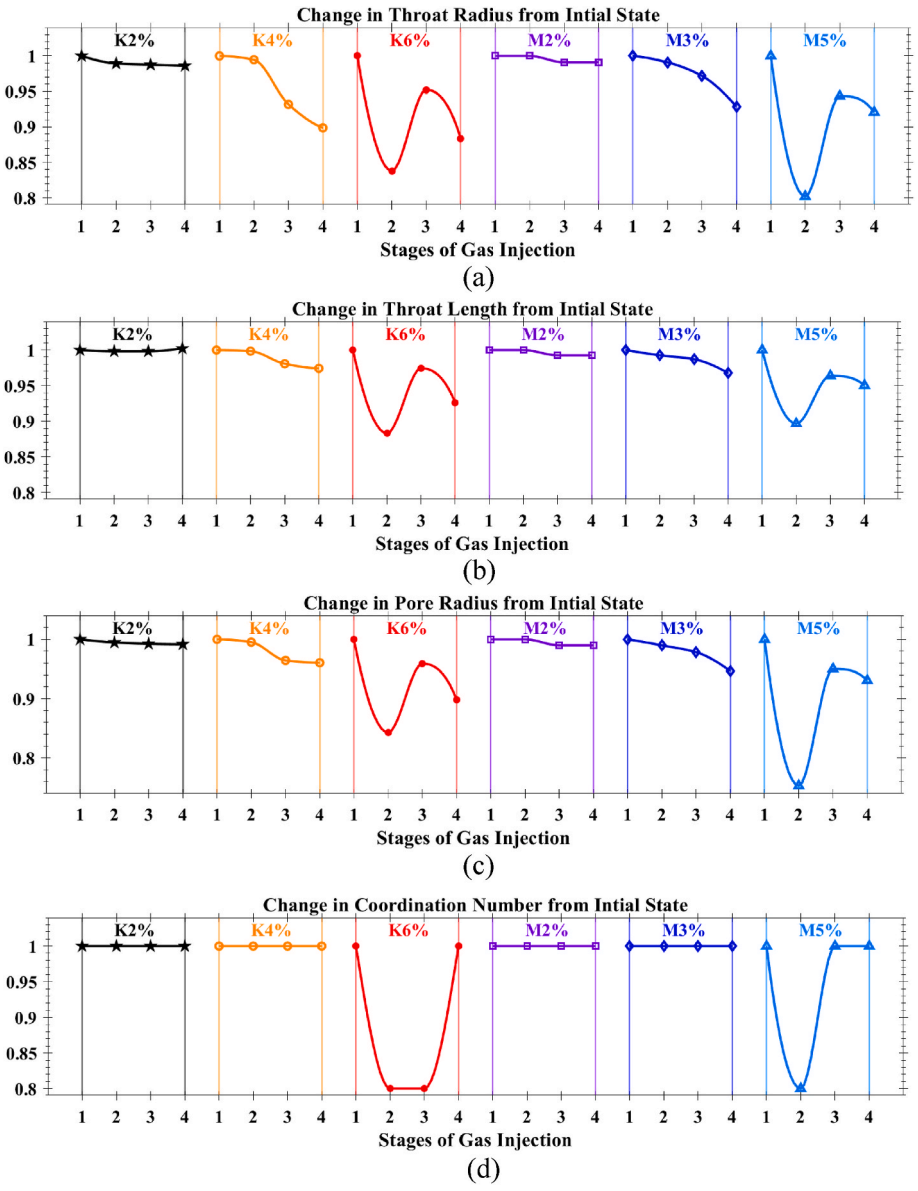

Fig. 7. Change in pore network properties for throats and pores from the initial stage for each system, showing the change over the 4 gas injection stages. (a) Is the mean throat radius, (b) the mean throat length, (c) the mean pore radius, and (d) the mean coordination number (connected throats to a pore).

surfaces which will increase with drainage. When the content of fines on the brine-water interface is low no dislocations in the sand will occur, but as the content increase, fines will bridge and clog the throats, causing the gas interface to push and displace sand grains.

Fig. 13 presents a visualization of the segmented gas phase after the final injection stage for kaolinite and montmorillonite samples, each separate ganglion is labeled with a different color. For the kaolinite samples, the flow pattern changed from capillary fingering to stable displacement and finally to fracturing, as the content of the fine changed from 2% (0.1FC*) to 4% (0.19FC*) and finally to 6% (0.28FC*) respectively. In the 6% kaolinite sample, the largest gas ganglion is represented in green filling the fractured body. Hydrophobic fines flowing through hydrophilic media, with contents above 5% can accumulate at the brine-gas interface and clog the pores (Jung et al., 2017). Gas ganglia of the montmorillonite samples change from stable displacement to disconnected flow to finally disconnected vuggy flow as the fines content increases from 2% (0.22FC*) to 3% (0.33FC*) and finally to 5% (0.55FC*) respectively. The hydrophilic nature of montmorillonite caused fines to accumulate at the gas-brine interface, which resulted in entrapping and detaching the gas ganglia (snap-off). Multiple detached volumes of CO_2 are shown in Fig. 13-M5%, where disconnected large vuggy pores were formed due to clogging, because the brine-gas interface of ganglia displaced the sand grains. Such observations agree with the findings of Primkulov et al. (2021) who developed a model based on Lenormand's phase diagram, initially the flow pattern is capillary, then as throats widen (via microfractures and vugs), the flow regime change respectively toward stable displacement and disconnected intermittent cooperate pore filling. Moreover, Osiptsov (2017) reported that a high ratio of fine particles is required to sustain fractured flow as in K6%, otherwise a fracture can collapse (Lee and Babadagli, 2021), which explains the disconnected vugs at M5%.

Fig. 14 utilizes the label measurements to illustrate the volume distribution of gas ganglia, after the final injection stage for all samples. At low fines contents (less than 4%), ganglia are fewer, larger and connected; mostly single body as seen in K2%, K4% and M2%. As fines content increases the gas bodies get divided and disconnected. For the montmorillonite sample with high fines content (5%), the number of disconnected ganglia is large, because of the formation of unconnected

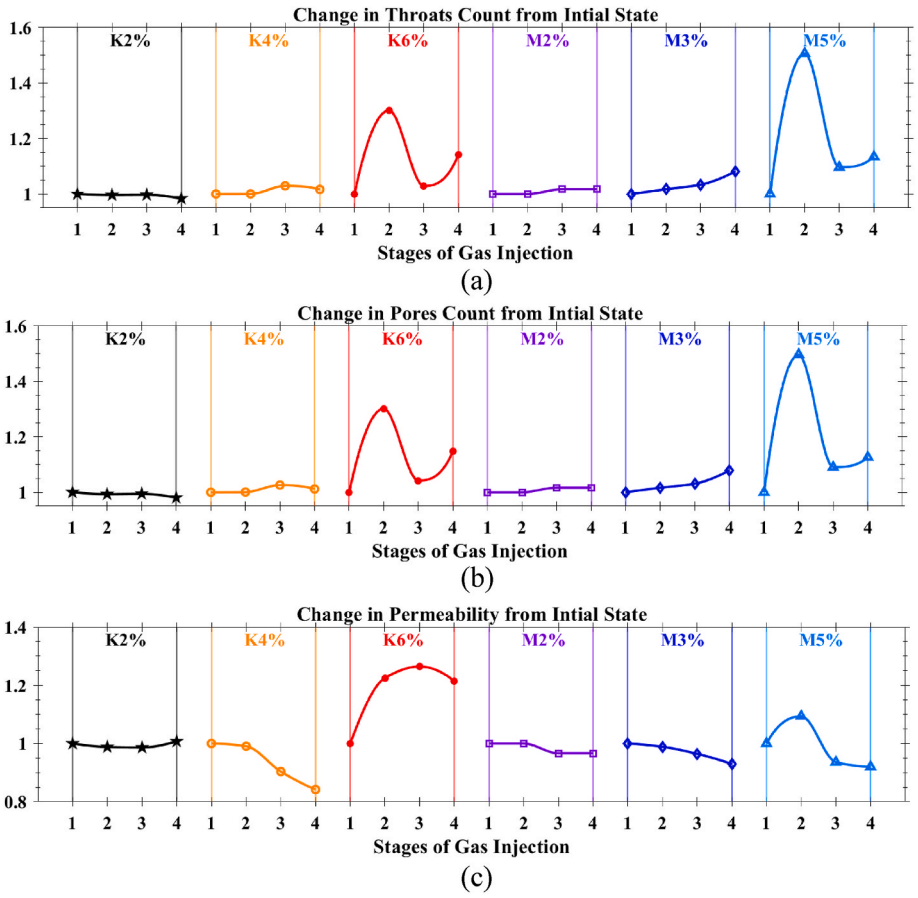

Fig. 8. Change in pore network properties and over permeability simulations from the initial stage for each system, showing the change over the 4 gas injection stages. (a) Is the number of throats, (b) the number of pores, and (c) single phase permeability through the pore network.

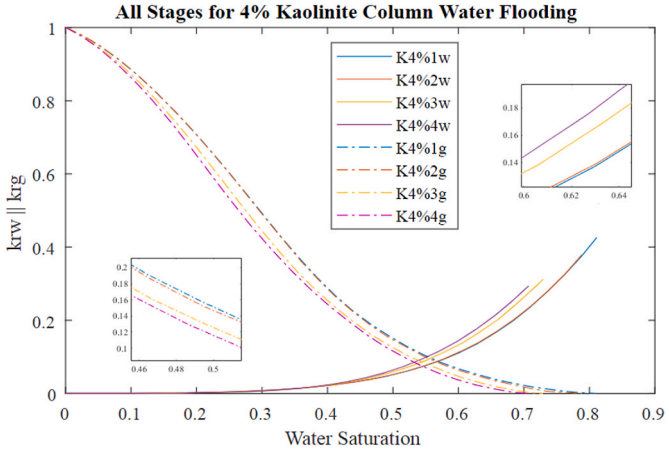

Fig. 9. Krw and krg Curves for All CO_2 Stages at 4% Kaolinite Column, Krw curves are solid while krg are dashed.

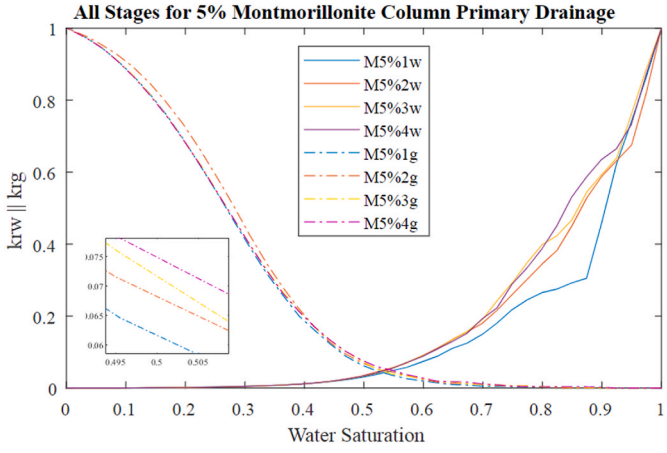

Fig. 10. Relative permeability of water krw and gas krg, for all CO_2 stages at 5% montmorillonite column.

vugs. Such disconnected vugs can lead to higher bottom well pressures which might impact hydrate equilibrium and therefore destabilize reservoir structure (Chibura et al., 2022). Meanwhile, for the 6% kaolinite sample, the ganglia stay connected with relatively larger volumes because of microfractures. This shows that small changes to the pore morphology of unconsolidated sandy sediments due to fines migration, can adversely affect the connectivity of gas flow. Opposite to observations of fines migration in consolidated rock samples, where small pore morphology deformations do not alter the connectivity of multiphase flow pathways (Hu et al., 2022).

Findings in this study provide guidance for safety and production teams that operate sandy reservoirs. Pore compression was universally observed for all systems due to gas injection, which induces multiphase flow causing fines migration that alters the pore morphology of sediments (Gu et al., 2022; Zhang et al., 2022). Regions near wellbores must be monitored as fines content typically increases radially with the flow direction toward a production well and outward an injection well. Findings reveal that hydrophobic clays (e.g., kaolinite) could contribute

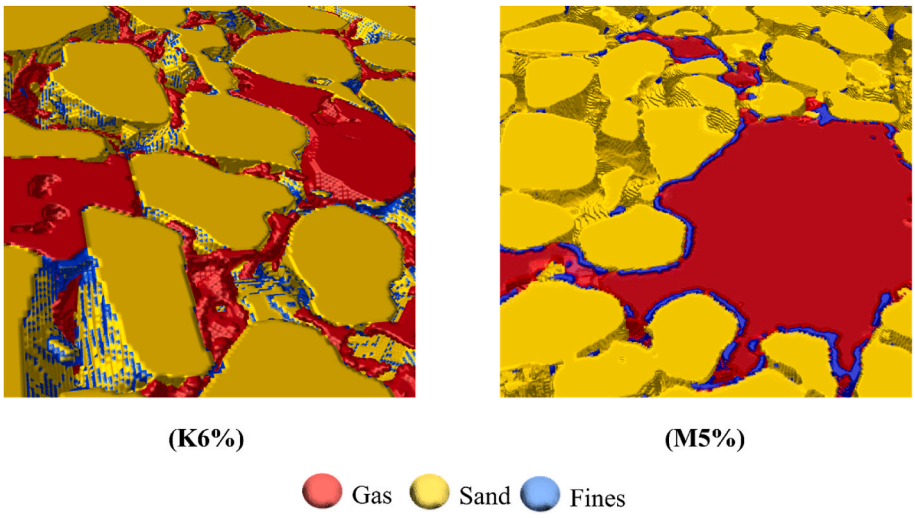

Fig. 11. 2D sections obtained from 3D tomography, hydrophobic kaolinite fines are observed at the sand-brine and brine-gas interfaces, while hydrophilic montmorillonite fines are observed at the brine-gas interface.

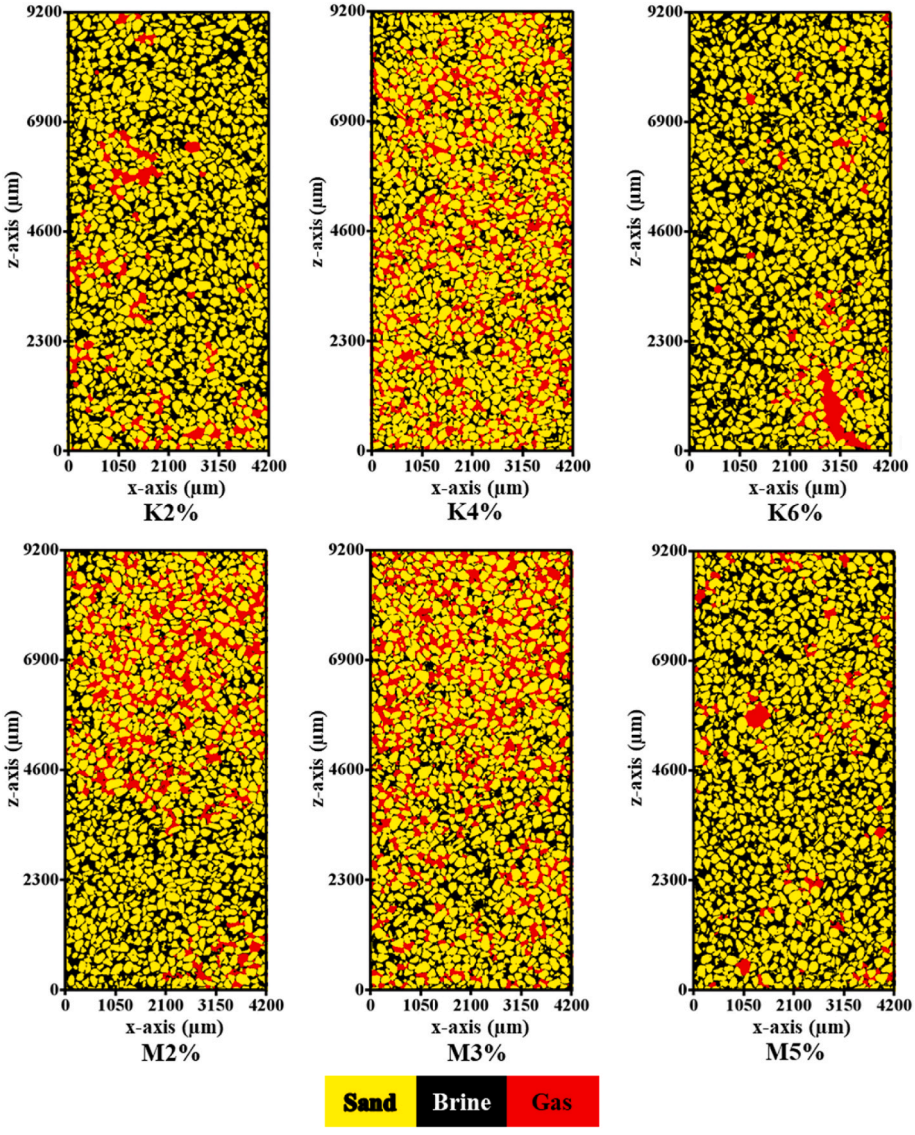

Fig. 12. Segmented images of 2D vertical cross sections, for all samples at the final CO_2 injection stage. As fines content increase beyond 4%, dislocations in sand grains develop, reducing the gas percolation to few pathways as in M5% or to a single path as in K6% (microfracture).

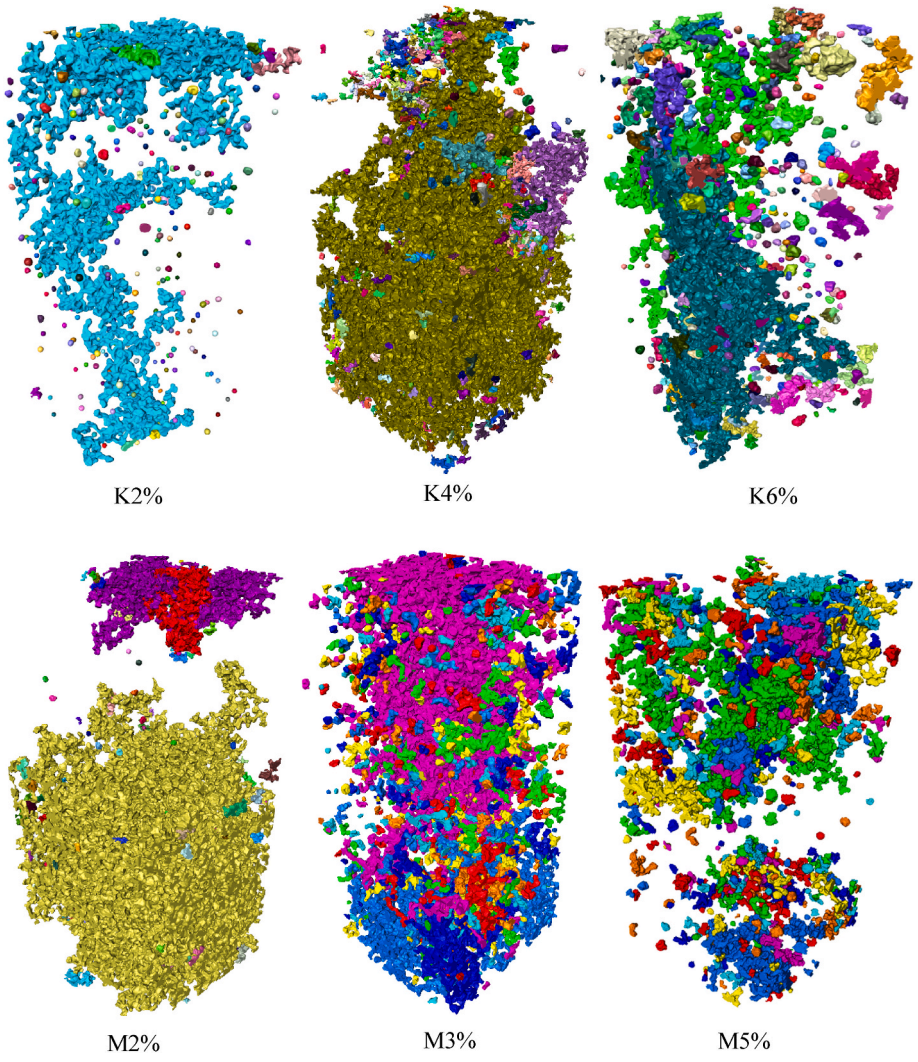

Fig. 13. 3D visualization of segmented gas phase at the final injection stage, each separate ganglion is labeled with a different color. In systems with kaolinite, gas flows in a connected body, as fines content increase the flow regime shifts from capillary to filling fracture body; while for montmorillonite the gas flow regime shifts from connected to disconnected vuggy flow.

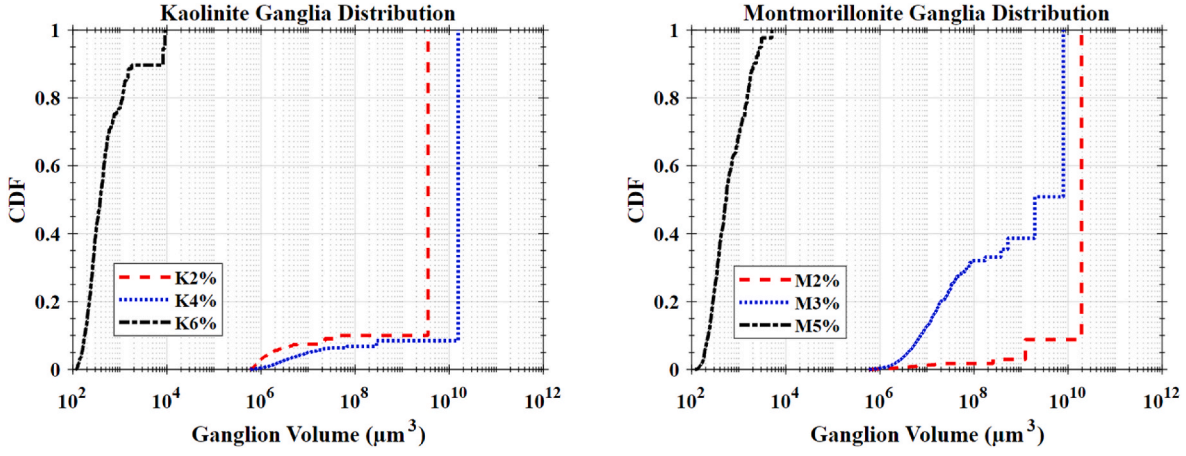

Fig. 14. Distributions of the volume of gas ganglia at the final injection stage for all samples, as the fines content rises the number of disconnected ganglia increases for montmorillonite, whereas for kaolinite the ganglia stay connected with relatively larger volumes because of microfractures. At low fines contents, ganglia are fewer, large and connected, mostly single body as seen in K2%, K4% and M2%.

to the formation of gas-induced fractures within sediments whereas hydrophilic clays (e.g., montmorillonite) could contribute to the formation of gas-induced vugs within sediments. This applies to vertical wellbore regions along with reservoir regions above large horizontal fracture networks. The presence of fines content of 6% kaolinite (0.28FC*) or 5% montmorillonite (0.55FC*) is shown to cause structural instability and may contribute to catastrophic geomechanical failure, especially in shutoff events (Zhang et al., 2022). This is a crucial observation for developing safety regulations for sandy reservoirs that commonly inhabit hydrates (Cook and Malinverno, 2013). For production teams, kaolinite is shown to lead to more connected gas flow through fractures, while montmorillonite resulted in disconnected intermittent gas flow due to the formation of disconnected vugs.

Limitations of this work include the use of repacked sand to simulate sediments, and the use of tomography which has a limited field of view at a specific resolution. Another limitation is the difference in the driving forces behind fines migration induced by dissociated hydrate gas and injected CO_2. Although both include a multiphase flow of gas and water along with the subsequent sweeping of the fluids interface, the difference is manifested in the presence of hydrate as a phase. The hydrate phase provides support to sediments by carrying the overhead stress and providing adhesion, limiting grains movement and restricting the void space for fluids to flow through. The experiments in this work depict the case in which hydrates have dissociated throughout a region in the reservoir, studying how gas flow at sediments with low confinement pressure couples with fines migration to change the pore morphology.

4. Conclusions

The effect of fines on pore morphology and gas connectivity was studied using unconsolidated sandy porous media. F75 silica sand was mixed with kaolinite and montmorillonite at different percentages by weight. It was then loosely packed in acrylic columns in five layers. The columns initially were fully saturated with KI brine. The 3D reconstruction was performed on saturated samples and after steps of CO_2 gas injection. The acquired 3D images were filtered and segmented, pore networks and permeability were simulated. The findings showed:

1 Generally, as fines content increases, the extent of deformation to pore morphology increases as gas flow induces fines migration. While higher fines contents result in skewing throat radii distribution toward lower throat sizes and higher throat numbers, indicating that throats get divided due to fines migration and clogging.
2 Montmorillonite clay generates vuggy pores with a detached gas ganglion; while the kaolinite fines induce the development of microfractures with connected main gas branches; these phenomena are observed at 5% montmorillonite and 6% kaolinite.
3 At low to middle fines content (i.e., $<$0.28FC* for kaolinite and $<$0.55FC* for montmorillonite), the mean throat radius gradually decreases. While samples with high fines content, a rapid drop in throat dimensions is observed after CO_2 injection.
4 The fines present in the system whether hydrophobic or hydrophilic reduced the throat diameters, due to dislocations in the sand grains.
5 Using direct observations from the tomography images, hydrophobic particles were observed at both sand-brine and brine-gas interfaces, while hydrophilic clay was observed at the brine-gas interface.
6 Using pore networks and permeability simulations indicated quantitative and qualitative changes in the sand pore morphology under low confinement pressure. The presence of low contents of fines in sandy media generally reduces throat radii during gas injection, until the content is high enough to induce clogging,
7 When clogging occurs due to fines migration from the gas injection, sand dislocations and fractures open the main flow pathway for gas, temporarily increasing the average throat radius of the pore network; until again more fines migrate and start to reduce the network average throat radius.
8 For kaolinite, the gas flow pattern changed from capillary fingering to stable displacement to finally fracturing, as the content of the fine changed from 0.1FC* to 0.19FC* and finally to 0.28FC*, respectively. While gas ganglia of montmorillonite samples change from stable displacement to disconnected flow to finally disconnected vuggy flow as the fines content increases from 0.22FC* to 0.33FC* and finally to 0.55FC*, respectively.

Credit authors statement

Conceptualization: Riyadh Al-Raoush, Khalid Alshibli, Jongwon Jung; Data curation: Riyadh Al-Raoush, Khalid Alshibli, Zaher Jarrar; Formal analysis: Jamal Hannun, Zaher Jarrar; Funding acquisition: Riyadh Al-Raoush, Khalid Alshibli, Jongwon Jung; Investigation: Jamal Hannun, Riyadh Al-Raoush, Khalid Alshibli, Jongwon Jung; Methodology: Riyadh Al-Raoush, Jamal Hannun, Zaher Jarrar , Khalid Alshibli; Project administration: Riyadh Al-Raoush, Khalid Alshibli, Jongwon Jung; Resources: Riyadh Al-Raoush, Khalid Alshibli, Jongwon Jung; Software: Riyadh Al-Raoush, Jamal Hannun, Zaher Jarrar; Supervision: Riyadh Al-Raoush; Validation: Jamal Hannun; Visualization: Jamal Hannun; Writing - original draft: Jamal Hannun; Writing - review and editing: Riyadh Al-Raoush Khalid Alshibli, Jongwon Jung, Zaher Jarrar.

Declaration of competing interest

The authors declare that they have no known competing financial interests or personal relationships that could have appeared to influence the work reported in this paper.

Data availability

Data will be made available on request.

Acknowledgments

Open Access funding provided by the Qatar National Library. This research was made possible by the National Priorities Research Program (NPRP) (grant # NPRP8-594-2-244) and the Graduate Sponsorship Research Award (GSRA) (grant # GSRA7-1-0217-20002) from Qatar National Research Fund (a member of Qatar Foundation). The findings achieved herein are solely the responsibility of the authors. The SMT images were collected using the X-ray Operations and Research Beamline Station 13-BMD at Argonne Photon Source (APS), Argonne National Laboratory. The authors thank Dr. Mark Rivers of APS for help in performing the SMT scans. The authors thank Dr. Wadi Imseeh for his help in performing the SMT scans. The authors also acknowledge the support of GeoSoilEnviroCARS (Sector 13), which is supported by the National Science Foundation, USA, Earth Sciences (EAR-1128799), and the US Department of Energy (DOE), Geosciences (DE-FG02-94ER14466). Use of the Advanced Photon Source, an Office of Science User Facility operated for the DOE Office of Science by Argonne National Laboratory, was supported by DOE, USA under (contract no. DE-AC02-06CH11357). The authors thank the reviewers for their suggestions and constructive comments that helped improve and enhance the manuscript.

References

Al-Raoush, R., 2012. Change in microstructure parameters of porous media over representative elementary volume for porosity. Part. Sci. Technol. 30 (1), 1–16. https://doi.org/10.1080/02726351.2010.543262.

Al-Raoush, R.I., Willson, C.S., 2005. A pore–scale investigation of a multiphase porous media system. J. Contam. Hydrol. 77 (1–2), 67–89. https://doi.org/10.1016/J.JCONHYD.2004.12.001.

Al-Raoush, R., Hannun, J., Jarrar, Z., Alshibli, K., Jung, J., 2019. Impact of fines type on gas flow using 3D micro-computed tomography. In: SPE Kuwait Oil & Gas Show and Conference. Society of Petroleum Engineers. https://doi.org/10.2118/198106-MS.

Alshibli, K.A., Druckrey, A.M., Al-Raoush, R.I., Weiskittel, T., Lavrik, N.V., 2015. Quantifying morphology of sands using 3D imaging. J. Mater. Civ. Eng. 27 (10) https://doi.org/10.1061/(ASCE)MT.1943-5533.0001246.

Andrew, M., Bijeljic, B., Blunt, M.J., 2014. Pore-scale contact angle measurements at reservoir conditions using X-ray microtomography. Adv. Water Resour. 68, 24–31. https://doi.org/10.1016/j.advwatres.2014.02.014.

Bakke, S., Øren, P.-E., 1997. 3-D pore-scale modelling of sandstones and flow simulations in the pore networks. SPE J. 2 (2), 136–149. https://doi.org/10.2118/35479-pa.

Bakke, S., Øren, P.-E., 2002. Process based reconstruction of sandstones and prediction of transport properties. Transport Porous Media 46 (2–3), 311–343. https://doi.org/10.1023/a:1015031122338.

Bate, B., Chen, C., Liu, P., Zhou, C., Chen, X., Nie, S., et al., 2022. The migration and deposition behaviors of montmorillonite and kaolinite particles in a two-dimensional micromodel. Materials 15, 855. https://doi.org/10.3390/MA15030855, 2022 Page 855, 15(3).

Bizmark, N., Schneider, J., Priestley, R.D., Datta, S.S., 2020. Multiscale dynamics of colloidal deposition and erosion in porous media. Sci. Adv. 6 (46), 2530–2543. https://doi.org/10.1126/SCIADV.ABC2530/SUPPL_FILE/ABC2530_SM.PDF.

Boswell, R., Collett, T.S., Frye, M., Shedd, W., McConnell, D.R., Shelander, D., 2012. Subsurface gas hydrates in the northern Gulf of Mexico. Mar. Petrol. Geol. 34 (1), 4–30. https://doi.org/10.1016/j.marpetgeo.2011.10.003.

Byrne, Michael, 2012. Formation Damage – Any Time, Any Place, Any where. http://www.afes.org.uk/uploads/files/Formation%20Damage%20%E2%80%93%20Any%20Time.pdf.

Chibura, P.E., Zhang, W., Luo, A., Wang, J., 2022. A review on gas hydrate production feasibility for permafrost and marine hydrates. J. Nat. Gas Sci. Eng. 104441. https://doi.org/10.1016/j.jngse.2022.104441.

Cook, A.E., Malinverno, A., 2013. Short migration of methane into a gas hydrate-bearing sand layer at Walker Ridge, Gulf of Mexico. G-cubed 14 (2), 283–291. https://doi.org/10.1002/ggge.20040.

Coronado, M., Díaz-Viera, M.A., 2017. Modeling fines migration and permeability loss caused by low salinity in porous media. J. Petrol. Sci. Eng. 150, 355–365. https://doi.org/10.1016/J.PETROL.2016.12.021.

Crist, J.T., Zevi, Y., McCarthy, J.F., Throop, J.A., Steenhuis, T.S., 2005. Transport and retention mechanisms of colloids in partially saturated porous media. Vadose Zone J. 4 (1), 184–195. https://doi.org/10.2113/4.1.184.

Deer, W.A., William, A., Howie, R.A., Robert, A., Zussman, J., 1992. An Introduction to the Rock-Forming Minerals. Longman Scientific & Technical.

Elrahmani, A., Al-Raoush, R.I., Abugazia, H., Seers, T., 2022. Pore-scale simulation of fine particles migration in porous media using coupled CFD-DEM. Powder Technol. 398, 117130 https://doi.org/10.1016/J.POWTEC.2022.117130.

Fei, 2020. PerGeos. Version 2020) FEI. http://www.thermofisher.com/pergeos.

Finlay, S., Marquez, X., Solling, T., Bounoua, N., Gagigi, T., 2014. Multi-scale carbonate reservoir characterisation and artificial neural networks reveals complexity in the shuaiba reservoir, Al shaheen field. In: International Petroleum Technology Conference.. https://doi.org/10.2523/IPTC-17639-MS

Golparvar, A., Zhou, Y., Wu, K., Ma, J., Yu, Z., 2018. A comprehensive review of pore scale modeling methodologies for multiphase flow in porous media. Advances in Geo-Energy Research 2 (4), 418–440. https://doi.org/10.26804/ager.2018.04.07.

Gu, Y., Sun, J., Qin, F., Ning, F., Li, Y., Cao, X., Liu, T., Wang, R., Jiang, G., 2022. Numerical analysis on gas production from silty hydrate reservoirs in the South China sea by depressurizing: the effect of permeability reduction caused by pore compression. J. Nat. Gas Sci. Eng. 104, 104680 https://doi.org/10.1016/J.JNGSE.2022.104680.

Guo, P., Tian, Z., Zhou, R., Chen, F., Du, J., Wang, Z., Hu, S., 2022. Chemical water shutoff agents and their plugging mechanism for gas reservoirs: a review and prospects. J. Nat. Gas Sci. Eng. 104, 104658 https://doi.org/10.1016/J.JNGSE.2022.104658.

Ham, K., Jin, H., Al-Raoush, R., Xie, X., Willson, C.S., Byerly, G.R., Simeral, L.S., Rivers, M.L., Kurtz, R.L., Butler, L.G., 2004. Three-dimensional chemical analysis with synchrotron tomography at multiple X-ray energies: brominated aromatic flame retardant and antimony oxide in polystyrene. Chem. Mater. 16 (21), 4032–4042. https://doi.org/10.1021/cm0350333.

Han, G., Kwon, T.-H., Lee, J.Y., Kneafsey, T.J., 2018. Depressurization-induced fines migration in sediments containing methane hydrate: X-ray computed tomography imaging experiments. J. Geophys. Res. Solid Earth 123 (4), 2539–2558. https://doi.org/10.1002/2017JB014988.

Hannun, J., Al-Raoush, R., Jarrar, Z., Alshibli, K., Jung, J., 2020. Use of 3D Images to Evaluate Formation Damage Induced by Montmorillonite Fines in Porous Media Systems. Qatar University, pp. 644–648. https://doi.org/10.29117/cic.2020.0082.

Hu, C., Jia, Y., Duan, Z., 2022. Pore and permeability properties of reservoir sandstone under a uniaxial compression CT test. J. Nat. Gas Sci. Eng. 104, 104666 https://doi.org/10.1016/J.JNGSE.2022.104666.

Iglauer, S., Paluszny, A., Blunt, M.J., 2013. Erratum: Simultaneous Oil Recovery and Residual Gas Storage: A Pore-Level Analysis Using in Situ X-Ray Micro-tomography. Fuel, pp. 905–914. https://doi.org/10.1016/j.fuel.2014.09.031. Fuel (2013.

Jang, J., Cao, S.C., Stern, L.A., Waite, W.F., Jung, J., Lee, J.Y., 2020. Potential freshening impacts on fines migration and pore-throat clogging during gas hydrate production: 2-D micromodel study with Diatomaceous UBGH2 sediments. Mar. Petrol. Geol. 116, 104244 https://doi.org/10.1016/j.marpetgeo.2020.104244.

Jarrar, Z.A., Al-Raoush, R.I., Hannun, J.A., Alshibli, K.A., Jung, J., 2020. 3D synchrotron computed tomography study on the influence of fines on gas driven fractures in Sandy Sediments. Geomechanics for Energy and the Environment, 23,, 100105. https://doi.org/10.1016/j.gete.2018.11.001.

Jarrar, Z.A., Alshibli, K.A., Al-Raoush, R.I., Jung, J., 2019. Gas driven fracture during gas production using 3D synchrotron computed tomography. In: Springer Series in Geomechanics and Geoengineering. https://doi.org/10.1007/978-3-319-99670-7_43.

Jarrar, Z.A., Al-Raoush, R.I., Hannun, J.A., Alshibli, K.A., 2021. New model for estimating geometric tortuosity of variably saturated porous media using 3D synchrotron microcomputed tomography imaging. Soil Sci. Soc. Am. J. 85 (6), 1867–1879. https://doi.org/10.1002/saj2.20289.

Jung, J.W., Jang, J., Santamarina, J.C., Tsouris, C., Phelps, T.J., Rawn, C.J., 2012a. Gas production from hydrate-bearing sediments: the role of fine particles. In: Energy and Fuels, vol. 26. American Chemical Society, pp. 480–487. https://doi.org/10.1021/ef101651b.

Jung, J.W., Jang, J., Santamarina, J.C., Tsouris, C., Phelps, T.J., Rawn, C.J., 2012b. Gas production from hydrate-bearing sediments: the role of fine particles. Energy Fuels 26 (1), 480–487. https://doi.org/10.1021/ef101651b.

Jung, J., Cao, S.C., Shin, Y.H., Al-Raoush, R.I., Alshibli, K., Choi, J.W., 2017. A microfluidic pore model to study the migration of fine particles in single-phase and multi-phase flows in porous media. Microsyst. Technol. 24 (2), 1071–1080. https://doi.org/10.1007/S00542-017-3462-1, 2017 24:2.

Jung, J., Cao, S.C., Shin, Y.-H., Al-Raoush, R.I., Alshibli, K., Choi, J.-W., 2018. A microfluidic pore model to study the migration of fine particles in single-phase and multi-phase flows in porous media. Microsyst. Technol. 24 (2), 1071–1080. https://doi.org/10.1007/s00542-017-3462-1.

Kajiyama, S., Hyodo, M., Nakata, Y., Yoshimoto, N., Wu, Y., Kato, A., 2017. Shear behaviour of methane hydrate bearing sand with various particle characteristics and fines. Soils Found. 57 (2), 176–193. https://doi.org/10.1016/j.sandf.2017.03.002.

Khan, Hasan Javed, 2016. Improved Permeability Estimation of Formation Damage through Imaged Core Flooding Experiments. University of Texas at Austin. Retrieved from. https://repositories.lib.utexas.edu/handle/2152/47001.

Khan, Hasan J., Mirabolghasemi, M.S., Yang, H., Sa Prodanovi, M., Dicarlo, D.A., Balhoff, M.T., 2017. Study of formation damage caused by retention of bi-dispersed particles using combined pore-scale simulations and particle flooding experiments. J. Petrol. Sci. Eng. 158, 293–308. https://doi.org/10.1016/j.petrol.2017.08.061.

Khan, Hasan Javed, DiCarlo, D., Prodanović, M., 2020. The effect of vug distribution on particle straining in permeable media. J. Hydrol. 580, 124306 https://doi.org/10.1016/J.JHYDROL.2019.124306.

Klauda, J.B., Sandler, S.I., 2005. Global distribution of methane hydrate in ocean sediment. Energy Fuel. 19 (2), 459–470. https://doi.org/10.1021/ef049798o.

Kvamme, B., 2015. Feasibility of simultaneous CO $_2$ storage and CH $_4$ production from natural gas hydrate using mixtures of CO $_2$ and N $_2$. Can. J. Chem. 93 (8), 897–905. https://doi.org/10.1139/cjc-2014-0501.

Lagasca, J.R.P., Kovscek, A.R., 2014. Fines migration and compaction in diatomaceous rocks. J. Petrol. Sci. Eng. 122, 108–118. https://doi.org/10.1016/J.PETROL.2014.06.024.

Lee, J., Babadagli, T., 2021. Effect of roughness on fluid flow and solute transport in a single fracture: a review of recent developments, current trends, and future research. J. Nat. Gas Sci. Eng. 91, 103971 https://doi.org/10.1016/j.jngse.2021.103971.

Malik, J., Perona, P., 1990. Scale-space and edge detection using anisotropic diffusion. IEEE Trans. Pattern Anal. Mach. Intell. 12 (7), 629–639. https://doi.org/10.1109/34.56205.

Merey, S., Al-Raoush, R.I., Jung, J., Alshibli, K.A., 2018. Comprehensive literature review on CH4-CO2 replacement in microscale porous media. J. Petrol. Sci. Eng. 171, 48–62. https://doi.org/10.1016/J.PETROL.2018.07.032.

Milkov, A.V., 2004. Global estimates of hydrate–bound gas in marine sediments: how much is really out there? Earth Sci. Rev. 66 (3–4), 183–197. https://doi.org/10.1016/j.earscirev.2003.11.002.

Mrozewski, S.A., Collett, T.S., Cook, A.E., Guerin, G., Zyrianova, M.V., Lee, M.W., Goldberg, D.S., 2011. Gulf of Mexico gas hydrate joint industry project leg II logging-while-drilling data acquisition and analysis. Mar. Petrol. Geol. 34 (1), 41–61. https://doi.org/10.1016/j.marpetgeo.2011.08.003.

Muecke, T.W., 1979. Formation fines and factors controlling their movement in porous media. J. Petrol. Technol. 31 (2), 144–150. https://doi.org/10.2118/7007-PA.

Nishad, S., Al-Raoush, R.I., 2021. Colloid retention and mobilization mechanisms under different physicochemical conditions in porous media: a micromodel study. Powder Technol. 377, 163–173. https://doi.org/10.1016/j.powtec.2020.08.086.

Nishad, S., Al-Raoush, R.I., Alazaiza, M.Y.D., 2021. Release of colloids in saturated porous media under transient hydro-chemical conditions: a pore-scale study. Colloids Surf. A Physicochem. Eng. Asp. 614, 126188 https://doi.org/10.1016/J.COLSURFA.2021.126188.

Oren, P.-E., Bakke, S., Arntzen, O.J., 2007. Extending predictive capabilities to network models. SPE J. 3 (4), 324–336. https://doi.org/10.2118/52052-pa.

Osiptsov, A.A., 2017. Fluid mechanics of hydraulic fracturing: a review. J. Petrol. Sci. Eng. 156, 513–535. https://doi.org/10.1016/j.petrol.2017.05.019.

Park, J., Santamarina, J.C., 2017. Revised soil classification system for coarse-fine mixtures. J. Geotech. Geoenviron. Eng. 143 (8), 04017039 https://doi.org/10.1061/(ASCE)GT.1943-5606.0001705.

Parvan, A., Jafari, S., Rahnama, M., Norouzi-Apourvari, S., Raoof, A., 2021. Insight into particle detachment in clogging of porous media; a pore scale study using lattice Boltzmann method. Adv. Water Resour. 151, 103888 https://doi.org/10.1016/J.ADVWATRES.2021.103888.

Pratt, W.K., 2014. Introduction to Digital Image Processing. CRC Press, Taylor & Francis Group.

Prempeh, K.O.K., Chequer, L., Badalyan, A., Bedrikovetsky, P., 2020. Effects of the capillary-entrapped phase on fines migration in porous media. J. Nat. Gas Sci. Eng. 73, 103047 https://doi.org/10.1016/J.JNGSE.2019.103047.

Primkulov, B., Pahlavan, A., Fu, X., Zhao, B., MacMinn, C., Juanes, R., 2021. Wettability and Lenormand's diagram. J. Fluid Mech. 923, A34. https://doi:10.1017/jfm.2021.579.

Ruspini, L.C., Farokhpoor, R., Øren, P.E., 2017. Pore-scale modeling of capillary trapping in water-wet porous media: a new cooperative pore-body filling model. Adv. Water Resour. 108, 1–14. https://doi.org/10.1016/j.advwatres.2017.07.008.

Russell, T., Pham, D., Neishaboor, M.T., Badalyan, A., Behr, A., Genolet, L., et al., 2017. Effects of kaolinite in rocks on fines migration. J. Nat. Gas Sci. Eng. 45, 243–255. https://doi.org/10.1016/J.JNGSE.2017.05.020.

Samari Kermani, M., Jafari, S., Rahnama, M., Raoof, A., 2020. Direct pore scale numerical simulation of colloid transport and retention. Part I: fluid flow velocity, colloid size, and pore structure effects. Adv. Water Resour. 144, 103694 https://doi.org/10.1016/J.ADVWATRES.2020.103694.

Schoderbek, D., Farrell, H., Howard, J., Raterman, K., Silpngarmlert, S., Martin, K., et al., 2013. ConocoPhillips Gas Hydrate Production Test. https://doi.org/10.2172/1123878. Pittsburgh, PA, and Morgantown, WV (United States).

Solling, T., Marquez, X., Finlay, S.J., Bounoua, N., Gagigi, T., McKay, T., Fogden, A., 2014. 3D imaging of the pore network in the shuaiba reservoir, Al shaheen field. In: International Petroleum Technology Conference.. https://doi.org/10.2523/IPTC-17673-MS

Song, W., Kovscek, A.R., 2016. Direct visualization of pore-scale fines migration and formation damage during low-salinity waterflooding. J. Nat. Gas Sci. Eng. 34, 1276–1283. https://doi.org/10.1016/J.JNGSE.2016.07.055.

Song, Y., Ranjith, P.G., Wu, B., Song, Z., 2021. A microscopic study of sand arches and sand skeletons under hydrodynamic force based on the CFD-DEM model. J. Nat. Gas Sci. Eng. 92, 104017 https://doi.org/10.1016/j.jngse.2021.104017.

Wan, J., Wilson, J.L., 1994. Colloid transport in unsaturated porous media. Water Resour. Res. 30 (4), 857–864. https://doi.org/10.1029/93WR03017.

Xiong, Q., Baychev, T.G., Jivkov, A.P., 2016. Review of pore network modelling of Porous Media: experimental Characterisations, network constructions and applications to reactive transport. J. Contam. Hydrol. 192, 101–117. https://doi.org/10.1016/j.jconhyd.2016.07.002.

Zhang, P., Zhou, Y., Liu, B., Deng, W., 2022. Multiphase flow model coupled with fine particle migration for applications in offshore gas hydrate extraction. J. Nat. Gas Sci. Eng. 102, 104586 https://doi.org/10.1016/J.JNGSE.2022.104586.